Catalysis Today 158 (2010) 12–21

Contents lists available at ScienceDirect

Catalysis Today

journal homepage: www.elsevier.com/locate/cattod

The effect of the Mo precursor on the nanostructure and activity of PtRuMo electrocatalysts for proton exchange membrane fuel cells

N. Tsiouvaras[a,b], M.A. Peña[a], J.L.G. Fierro[a], E. Pastor[b], M.V. Martínez-Huerta[a,*]

[a] Instituto de Catálisis y Petroleoquímica, CSIC, Marie Curie 2, Cantoblanco, 28049 Madrid, Spain
[b] Departamento de Química Física, Universidad de La Laguna, Astrofísico Francisco Sánchez s/n, 38071 Tenerife, Spain

ARTICLE INFO

Article history:
Available online 17 June 2010

Keywords:
PEMFC
DMFC
Electrocatalysts
Anode
PtRuMo
DEMS

ABSTRACT

Carbon supported PtRuMo nanoparticles for CO and methanol electrooxidation have been prepared using different Mo precursors ($MoCl_5$, $(NH_4)_6Mo_7O_{24}$ and MoO_3). Electrocatalysts as well as support characterization has been carried out through various physicochemical (XRD, TEM, XPS, TPR and TXRF) and electrochemical techniques as cyclic voltammetries and current–time curves, applied in combination with differential electrochemical mass spectrometry (DEMS). MoO_3 precursor was mainly used as representative of Mo^{6+} species in the electrocatalyst. The results of this work pointed out that irrespectively of the similar structure and particle size are obtained using $MoCl_5$ and $(NH_4)_6Mo_7O_{24}$, the final composition and homogeneity of the ternary catalysts were found to depend markedly on these precursors. $MoCl_5$ led to a dramatic loss of Mo, while $(NH_4)_6Mo_7O_{24}$ appeared to be more stable and handy for synthesis of PtRuMo nanoparticles. Once the catalysts have been stabilized in the electrode, similar Mo species, mainly Mo^{5+}, are formed on the catalysts surface of all PtRuMo catalysts. This is indicative that similar metal–support and metal–metal interactions are likely developed in carbon supported PtRuMo nanoparticles at these potential conditions. The possible metal interactions that take place and the lower oxidation states of surface Mo species may be responsible of the high activity in CO and methanol electrooxidation as compared with binary and ternary catalysts obtained with MoO_3. The higher activity observed using $(NH_4)_6Mo_7O_{24}$ as precursor could be finally attributed to the composition and a remarkable Ru–Mo interaction detected by TPR. Finally, the MoO_3-loaded catalyst proves that high oxidation states of Mo not only result in high losses of metals during the stabilization of the system and lower activities but also affect negatively the development of Pt–Ru interactions.

1. Introduction

Proton exchange membrane fuel cells (PEMFC), fed with H_2/CO or methanol in direct methanol fuel cells (DMFC), are recognized as very attractive devices to obtain directly electric energy via controlled oxidation of the fuel (H_2 or methanol). These cells operate at low temperatures (70–120 °C), present fast start-up and provide high energy densities. For this reason their use is considered ideal for any type of portable devices as well as for transport systems as cars [1,2].

The state of the art of anodic catalysts for this technology is binary catalysts based on carbon supported PtRu nanoparticles [3,4]. However, these bimetallic systems are costly and not efficient enough for its implementation. The main problem in these catalysts is the carbon monoxide (CO) poisoning. The low amounts of CO (ppm levels) present in the H_2 feed from reformate streams or as a by-product of the methanol electrooxidation, gradually passivate the Pt active sites of the PEMFCs electrocatalysts causing energy output drops that hinder the systems operation and efficiency. Oxidation of adsorbed CO is regarded as the rate-determining step, and Ru is widely accepted as a promoter for CO oxidation. Its function is commonly explained on the basis of the bifunctional mechanism [5] or the "ligand effect" [6] or a combination of the two.

Exploring ternary PtRuMo catalysts is one of the most interesting approaches for improving their performance [7–13]. Mo is a cheaper and more abundant transition metal than Pt and Ru, although Mo role has yet to be fully determined. Molybdenum oxide possesses thermodynamic characteristics that allow water discharge at low overpotentials [14], consequently the dissociation of water appears to be much easier on PtMo than on pure Pt [15]. Additionally, nonstoichiometric lower valence molybdenum oxides, called the Magneli phases, which have compositions between MoO_2 and MoO_3, have a rutile-type structure with short metal-metal bond distance along the direction of edge sharing, which accounts for the high electronic conductivity of these materials [16].

* Corresponding author. Tel.: +34 5854778; fax: +34 5854760.
E-mail address: mmartinez@icp.csic.es (M.V. Martínez-Huerta).

0920-5861/$ – see front matter © 2010 Elsevier B.V. All rights reserved.
doi:10.1016/j.cattod.2010.05.004

Recently, our team developed a new synthesis method of PtRu–MoO_x nanoparticles supported on carbon black and carbon nanofibres by a two-step procedure [13,17]. From differential electrochemical mass spectrometry (DEMS), a significant negative shift of about 0.2 V in the onset potential for CO_2 was established for PtRu–MoO_x nanoparticles supported on carbon with respect to commercial PtRu/C (Johnson Matthey) catalyst. However, structural characteristics as chemical state, degree of alloying, particle size and the stability of Mo in ternary PtRuMo/C systems are still unclear and more studies are necessary in order to further understand their full effect in the CO and methanol electrooxidation.

In the present work the effect of the Mo precursor on the activity for CO and methanol electrooxidation has been investigated. Different Mo precursors as $MoCl_5$, $(NH_4)_6Mo_7O_{24}$ and MoO_3 lead to the incorporation of different Mo phases such as Mo^{5+}, Mo^{6+} or Mo^{5+}/Mo^{6+} mixed phases. This can consequently alter the surface chemistry of nanoparticles and affect their electroactivity. For the analysis of the electrocatalysts structure, different physicochemical techniques have been employed such as photoelectron spectroscopy (XPS), X-ray diffraction (XRD), total-reflection X-ray fluorescence (TXRF), transmission electron microscopy (TEM) and temperature-programmed reduction (TPR). Electrocatalysts have been analyzed using conventional electrochemical techniques such as cyclic voltammetry and current–time curves applied in combination with differential electrochemical mass spectrometry (DEMS).

2. Experimental

2.1. Catalyst preparation

Vulcan XC-72R (Cabot Co.) was used as the support material. For the catalyst preparation a two-step procedure has been employed [13]. In a first step the carbon support was impregnated with the respective Mo precursor, and in a second step PtRu has been incorporated to the Mo/C supports following a colloidal technique.

For the synthesis of MoX/C supports (where X denotes Cl, NH or O), $MoCl_5$ (Aldrich), $(NH_4)_6Mo_7O_{24}$ (Aldrich) and MoO_3 (Aldrich) were used as precursors, respectively. The MoCl/C support was synthesized by dissolving molybdenum pentachloride in deionized water (>18 MΩ cm) to obtain a 100 mM Mo solution, which was then added to the carbon dispersed in methanol solution and kept under vigorous stirring. Tetramethylammonium hydroxide solution was then added dropwise to precipitate the hydrous molybdenum oxide on the carbon particles. After 1 h aging under stirring, the MoCl/C solid was recovered by filtration and dried at 110 °C for 17 h. The MoNH/C support was synthesized adding 300 mM of ammonium molybdate solution and 100 mM of H_2O_2 over carbon black. The solution was then stirred for 48 h at room temperature and dried at 110 °C for 17 h. The MoO/C support was synthesized adding 300 mM of MoO_3 solution and 100 mM of H_2O_2 over carbon black. The solution was then stirred for 48 h at room temperature and dried at 110 °C for 17 h.

In a second step, Pt and Ru metals were loaded on the MoCl/C, MoNH/C and MoO/C samples according to the colloidal methodology [18], to obtain an atomic ratio Pt:Ru:Mo of 1:1:1.3 for MoCl/C and MoNH/C supports and 1:1:3 for MoO/C support. The reaction was performed in water with aqueous solutions of reactants. The appropriate concentration of H_2PtCl_6 was reduced by adding a solution of $Na_2S_2O_5$ ($NaHSO_3$) to obtain a colorless soluble intermediate of platinum, which was then oxidized with H_2O_2 (30%, v/v). During addition the pH of the solution was adjusted to ca. 5 by adding Na_2CO_3. The appropriate amount of $RuCl_3$ solution was then added dropwise under continuous stirring while keeping the pH close to ca. 5. The required amount of Mo/C support was added to the colloidal solution under constant stirring. Hydrogen gas was bubbled through this admixture for 2 h, and then the suspension was allowed to settle, filtered, washed with hot water, and then dried in an air oven at 110 °C for 15 h. Three catalysts were prepared: PtRu/MoCl/C (labeled PRMCl), PtRu/MoNH/C (labeled PRMNH), and PtRu/MoO/C (labeled PRMO). For comparison purpose, a binary catalyst PtRu (1:1)/C (labeled PR), obtained following the same colloidal methodology [18] was also analyzed. Solutions were prepared using Millipore-MiliQ water and analytical-grade reagents.

2.2. Physicochemical characterization

Atomic ratio Pt/Ru/Mo of samples was determined by total-reflection X-ray fluorescence (TXRF). Analysis was performed on a Seifert EXTRA-II spectrometer equipped with two X-ray fine focus lines, Mo and W anodes and a Si(Li) detector with an active area of 80 mm^2 and a resolution of 157 eV at 5.9 keV (MnKα). The Pt/Ru atomic ratio was determined using Pt*L*α and Ru*L*α emission lines in the XRF spectra after proper calibration with standard samples.

Thermogravimetric analysis (TGA) under controlled atmosphere was carried out on a Mettler Toledo TGA/SDTA851e using 200 $cm^3\ min^{-1}$ of N_2 as carrier gas, 20 $cm^3\ min^{-1}$ of oxygen as reactive gas, and a heating rate of 10 °C min^{-1}.

Metal phases and crystalline particle size have been determined using X-ray diffraction (XRD) measurements. XRD powder patterns were obtained on a PANalytical X'Pert Pro X-ray diffractometer using a Cu Kα source. The diffraction profiles of the samples were recorded within Bragg's angles ranging from 2° to 90° at a scanning rate of 0.04° per sec. The average particle size was estimated according to the Scherrer' formula from the reflections of the (2 2 0) diffraction peak, face-centered cubic lattice parameter was also calculated from the Pt peaks in the XRD patterns.

Particle size and morphology were evaluated from the transmission electron microscopy (TEM) images obtained in a JEM 2100F microscope operated with an accelerating voltage of 200 kV. The standard procedure involved dispersing 4 mg of the sample in ethanol in an ultrasonic bath for 15 min. The sample was then placed on a Cu carbon grid where the liquid phase was evaporated.

The H_2 temperature-programmed reduction (H_2-TPR) experiments were run in a Micrometrics equipment model TPD/TPR 2900 fitted with a TCD detector. Samples of ca. 20 mg each were used. The TPR experiments were run in a 10% H_2/Ar stream, with a heating rate of 10 °C min^{-1} and 80 $cm^3\ min^{-1}$ flow rate.

X-ray photoelectron spectroscopy (XPS) analysis was used in order to get information on the chemical state and concentration of surface species. XP spectra were obtained with a VG Escalab 200R spectrometer equipped with a hemispherical electron analyzer (constant pass energy of 50 eV) and a MgKα ($h\nu$ = 1254.6 eV) X-ray source, powered at 120 W. The XPS data signals were taken in increments of 0.1 eV with dwell times of 50 ms. Binding energies were calibrated relative to the C 1s peak at 284.6 eV. High resolution spectra envelopes were obtained by curve fitting synthetic peak components using the software *XPS peak*. The raw data were used with no preliminary smoothing. Symmetric Gaussian–Lorentzian product functions were used to approximate the line shapes of the fitting components.

2.3. Electrochemical characterization

All solutions were prepared from Millipore Milli-Q* water and analytical-grade reagents. The electrolytic solutions employed were 0.5 M H_2SO_4 (98% Merck p.a.) for CO electrooxidation experiments and 2 M CH_3OH (99.98% Scharlau) in 0.5 M H_2SO_4 for methanol oxidation. Freshly prepared solutions were purged with Ar (99.998% Air Liquide).

Table 1
Physicochemical parameters of the samples based on the analysis of TXRF, TGA and XRD.

Catalysts	Nominal atomic ratio Pt:Ru:Mo	Experimental atomic ratio Pt:Ru:Mo	Total metal loading	Average particle size (nm)	Lattice parameter (a_{fcc}) (Å)
PRMCl	1:1:1.3	1:1:0.4	25	3.8 ± 0.5	3.890
PRMNH	1:1:1.3	1:1:1.2	19	3.9 ± 0.5	3.901
PRMO	1:1:3	1:1:2.9	27	2.7 ± 0.5	3.928
PR	1:1	1:0.9	16	3.2 ± 0.5	3.925

The electrochemical measurements were carried out at room temperature in a three-electrode cell connected to an electrochemical analyzer (Autolab PGstat 302N). First, the ink of the electrocatalysts was prepared dispersing 4 mg of the material in 1 mL of water and 30 μL of Nafion (5 wt.% Aldrich) in an ultrasonic bath for 30 min. Then 5 μL of the ink were deposited onto a glassy carbon electrodes (6.0 mm diameter) and dried in an Ar flow for 20 min. The counter electrode was glassy carbon. For stripping of CO and methanol current–time curves, Hg/Hg_2SO_4 was used as the reference electrode, although data in the paper are referenced to the reversible hydrogen electrode (RHE). A reversible hydrogen electrode (RHE) in the supporting electrolyte was employed as the reference electrode for differential electrochemical mass spectrometry (DEMS).

In all experiments, the working electrode was activated in the supporting electrolyte solution by potential cycling between 0.05 and 0.8 V and one cycle between 0.05 and 1.15 V. The anodic stripping of CO adsorbed was studied after bubbling the gas for 15 min while polarizing the electrode at 0.07 V. The potential was cycled in the 0.05–0.8 V versus RHE potential range at the sweep rate of 10 mV s^{-1}. Current–time curves of the electrocatalysts towards methanol oxidation were carried out at 0.6 V in 2 M CH_3OH in 0.5 M H_2SO_4. Current scale was normalized for the electrochemical active surface (EAS) estimated from CO_{ads} stripping voltammetry.

Differential electrochemical mass spectrometry (DEMS) experiments were carried out in a 2 cm^3 plexiglass flow cell directly attached to the vacuum chamber of the mass spectrometer (Balzers QMG112) provided with a Faraday cup detector. The experimental set-up allows the simultaneous acquisition of mass spectrometric cyclic voltammograms (MSCVs) for selected masses and conventional voltammograms (CVs) recorded at a scan rate of 0.005 V s^{-1}. The experimental details are described elsewhere [13].

3. Results and discussion

3.1. Structural characterization

Analytical results of samples using TXRF and TG techniques are compiled in Table 1. The combination of both TXRF and TG was necessary for calculation of metal loading of Pt, Ru, and Mo (wt%) since no reliable analysis of Ru was obtained by ICP [13]. Due to the fact that crystal phases of MoO_3 are easily dissolved into the electrolyte (0.5 M H_2SO_4) double amount of Mo was used with MoO_3 precursor with respect to other supports. This fact has not been considerate relevant since MoO/C and PRMO samples were mainly used as representative of MoO_3 species.

It can be seen in Table 1 that the incorporation of Pt and Ru by colloidal methodology decreases metal loading in all samples, which are lost along the filtration step. However, the experimental atomic ratio of Pt, Ru and Mo are analogous to the nominal value in PRMNH and PRMO catalysts, although loss of Mo in the synthesis is evident when $MoCl_5$ is used as precursor in PRMCl. This is due to the fact that there is a strong dependence of Mo on the pH of the solution, and Mo is solubilized as polyanions during the synthesis of MoCl/C. $MoCl_5$ reacts easily with water to give $MoOCl_3$, $MoO_2(OH)_2$ and HCl compounds, which decrease pH to values lower than 2. It is known that different Mo^{6+} species are formed depending on the pH of the solution, and namely at low pH water soluble species like $MoO_2(H_2O)_4^{2+}$ (pH = 0) and $MoO_3 \cdot xH_2O$ (pH = 2) are predominant in the system [19].

X-ray diffraction patterns of samples are shown in Fig. 1. The Vulcan XC 72R substrate shows the characteristic diffraction pattern of graphitic carbon. MoO/C presents diffraction peaks typical of crystalline MoO_3 (JPCDS 47-1320). The diffraction lines observed at $2\theta = 23.6^\circ$, 25.8°, 27.4°, 39.2°, and 39.3° are assigned to $d(1\,0\,1)$,

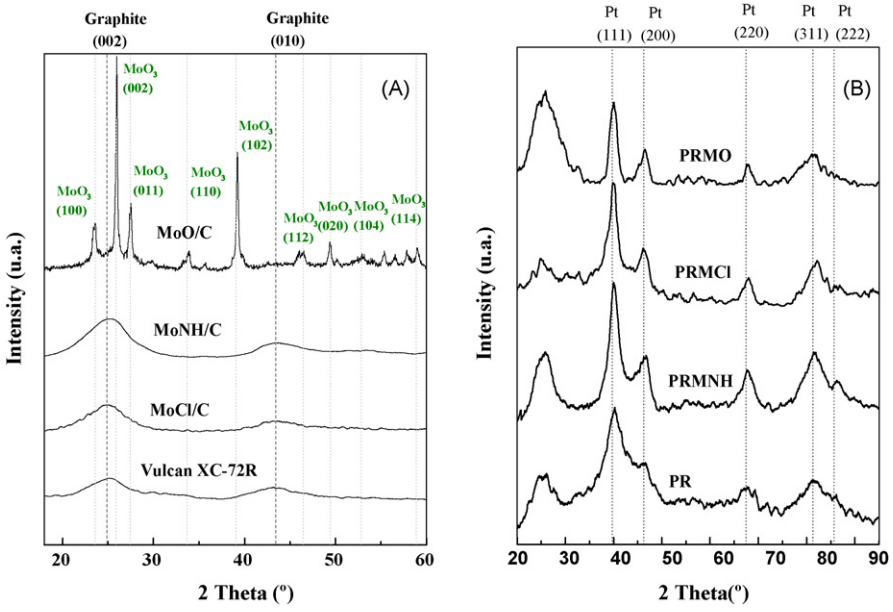

Fig. 1. X-ray diffraction of supports (A) and electrocatalysts (B).

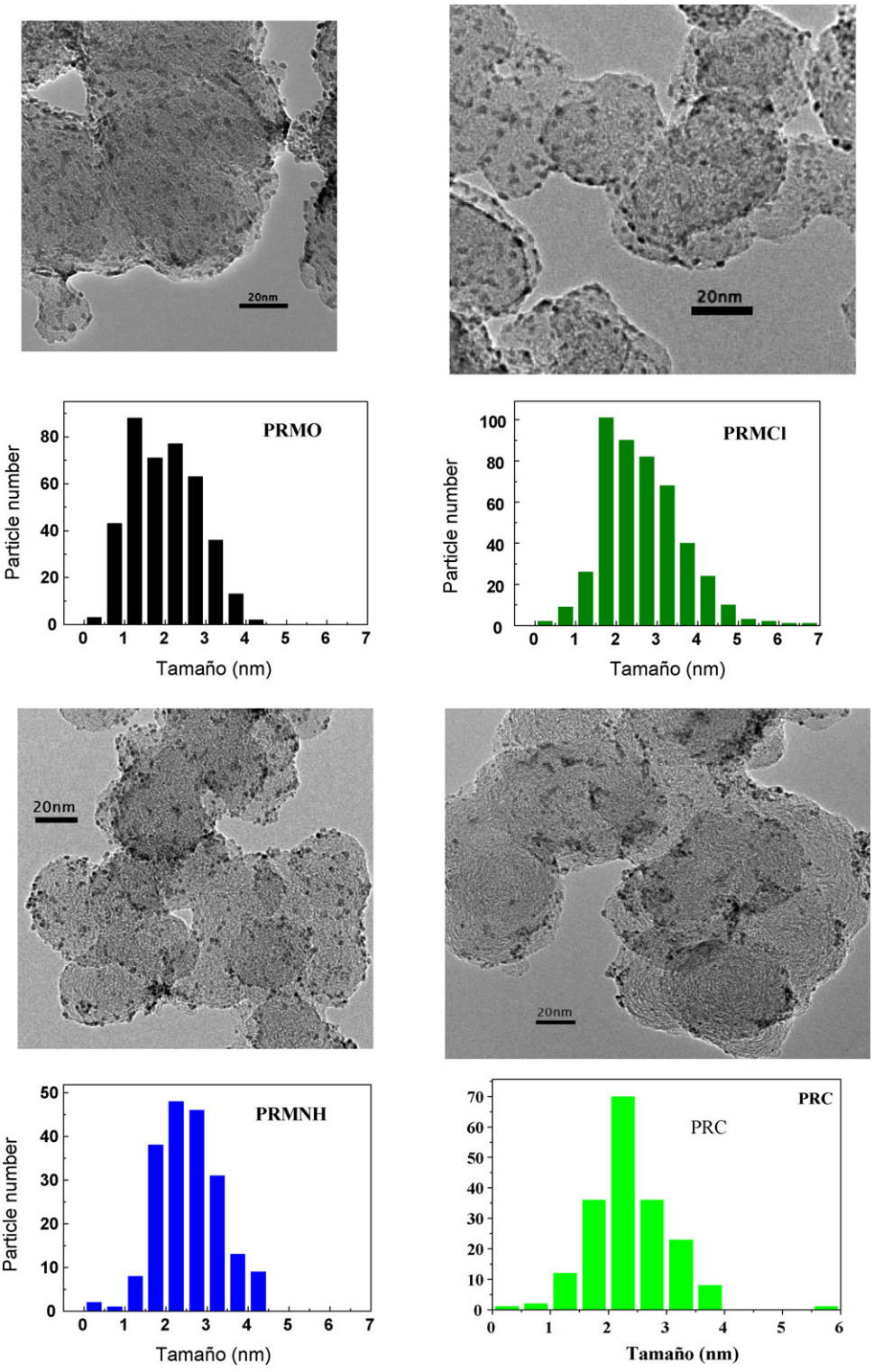

Fig. 2. TEM images of ternary catalysts.

$d(0\,0\,2)$, $d(0\,1\,1)$, $d(0\,0\,3)$, and $d(1\,1\,2)$ diffraction of the MoO_3 phase. The absence of these diffraction peaks in MoCl/C and MoNH/C could indicate that molybdenum species do not form crystalline aggregate, maintaining a good dispersion.

XRD patterns of the binary and ternary samples (Fig. 1B) show the characteristic diffraction lines of Pt^0 metal with a low degree of crystallinity and the absence of Mo, Ru and crystalline metals oxides. The average particle size was estimated according to the Scherrer's formula and the results are given in Table 1. The main crystal sizes were found to be in the nanoscale range of 2.7–3.9 nm for all catalysts. Lattice parameter has also been calculated in order to evaluate the level of PtRu alloying. Results point to a lower degree of alloying between Pt and Ru, which corresponds to an increase in the lattice constant compared to a solid solution of PtRu (3.83 Å) [20]. Pt and Mo have similar metallic radii, therefore the changes in lattice parameter in PtMo alloys are very small, making it imprac-

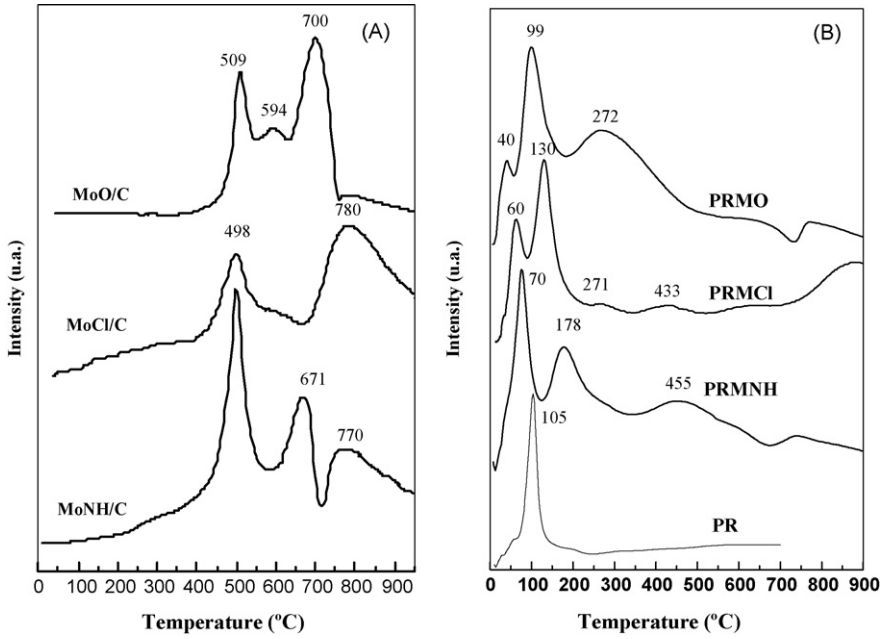

Fig. 3. TPR profiles of supports (A) and electrocatalysts (B).

tical to obtain a composition analysis of the possible alloy phases Pt, Ru or Mo in the supported catalysts.

Transmission electronic microscopy (TEM) images of binary and ternary catalysts are shown in Fig. 2. In general, there is a homogeneous distribution of the nanoparticles. The Mo precursor does not seem to affect to the average crystal size, which is in the order of 2–3 nm, and it is characteristic of all ternary samples.

TPR analysis of the Mo/C supports are presented in Fig. 3A and show different profiles depending on the precursor used. Though MoO/C shows similar diffraction lines to MoO_3, different TPR profile is observed in MoO/C with respect to MoO_3 (714, 780, 819 and 880 °C) [21]. In all supports the reduction of molybdenum oxides begins at temperature between 400 and 500 °C. However, different reduction peaks take place at higher temperature depending on the precursor, where several MoO_x suboxides can be formed. These results show that the reducibility of supported molybdenum oxides can be altered by the degree of Mo–support chemical interaction and the nature of the surface species developed during preparation of MoO/C sample.

Table 2
Binding energies (eV) of core levels of electrocatalysts and surface atomic ratio.

Samples	Binding energies (eV)			Surface metal weight (wt. %) Pt + Ru + Mo	Atomic ratio Pt:Ru:Mo
	$Pt4f_{7/2}$	$Ru3p_{3/2}$	$Mo3d_{5/2}$		
MoO_3			232.9 (100)		
MoO/C			232.2 (30) 233.1 (70)	12	
PRMO	71.7 (18) 72.9 (34) 74.8 (48)	463.7 (72) 466.3 (28)	232.2 (43) 233.2 (57)	45	1:1.7:2.4
$MoCl_5$			232.1 (75) 232.8 (25)		
MoCl/C			232.3 (54) 233.2 (46)	6	
PRMCl	71.7 (19) 72.8 (37) 74.8 (44)	463.6 (74) 466.5 (26)	232.2 (100)	30	1:1.3:0.4
$(NH_4)_6Mo_7O_{24}{\cdot}4H_2O$			232.2 (19) 232.8 (81)		
MoNH/C			232.3 (44) 233.1 (56)	7	
PRMNH	71.7 (20) 72.7 (45) 74.0 (35)	463.6 (77) 466.2 (23)	232.3 (78) 233.3 (22)	21	1:1.5:1.3
PR	71.6 (18) 72.7 (54) 74.9 (28)	463.5 (74) 465.6 (26)		24	1:1

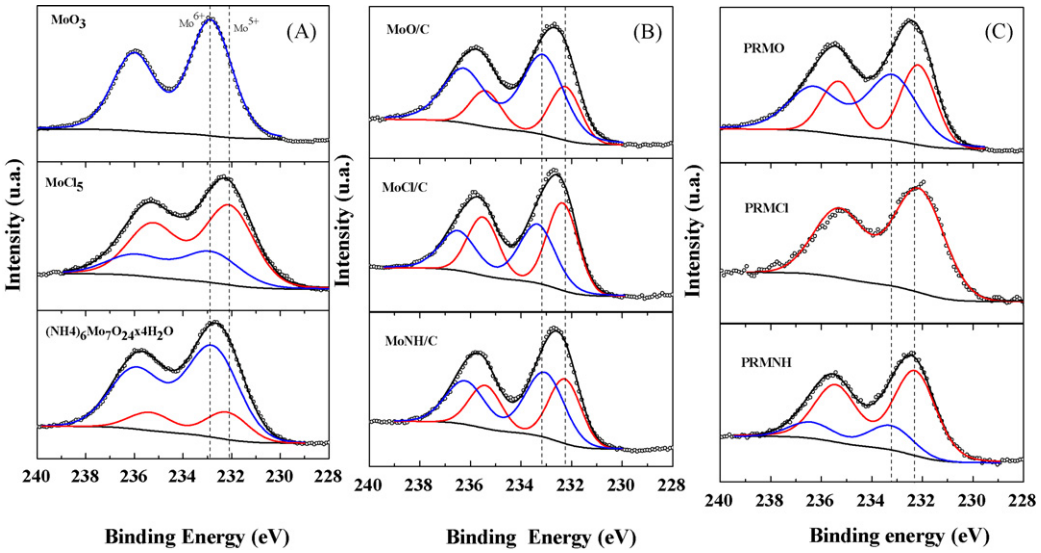

Fig. 4. Mo_{3d} core-level spectra of precursors (A), supports (B) and electrocatalysts (C).

Incorporation of Pt and Ru shifts the molybdenum oxide reduction peaks at lower temperatures (Fig. 3B). TPR peaks between 40 and 70 °C in ternary catalysts are due to partially oxidized platinum, and reduction peaks ca. 100 °C in PR and PRMO correspond to a RuO_xH_y species [22]. A shift of this reduction peak at higher temperatures in PRMCl (130 °C) and in PRMNH (178 °C) could be due to a direct interaction or a stabilization of oxidation states between Ru and Mo. The other peaks in PRMO, PRMCl, and PRMNH are assigned to molybdenum oxide species, although the precise phases have not yet been established. Thus, the incorporation of Pt and Ru by the colloidal method can substantially change the coordination of molybdenum oxide, and different MoO_x phases are formed depending on the precursor. Accordingly, the ability of Pt metal nanoparticles to enhance reduction of metal transition oxides by hydrogen via spillover processes is considered [23,24].

The nature of metal surface species of the samples was investigated by XPS analysis. Both binding energies of core levels and surface atomic ratios are given in Table 2. The Pt 4f signal doublets in all samples are derived from three pairs of Pt species, which are attributed to metallic Pt^0 nanoparticles (71.6-71.7 eV), Pt^{2+} species in PtO and $Pt(OH)_2$-like species (72.7–72.9 eV) and Pt^{4+} (74.0–74.9 eV) [25]. Similar concentrations of Pt species were found in electrocatalysts, except for binary catalyst, where the contribution of Pt^{4+} decreased. The Ru $3p_{3/2}$ signal of samples derives of two species in similar concentrations in all catalysts assigned to Ru^{4+} in anhydrous RuO_2 (463.5–463.7 eV) and hydrous amorphous $RuO_2{\cdot}xH_2O$ species (465.6–466.5 eV) [26].

The binding energy of the Mo $3d_{5/2}$ component of MoO_3 at 232.9 eV is typical of Mo^{6+} [25] (Fig. 4). However, incorporation of MoO_3 on the carbon substrate results in a partial reduction of Mo^{6+} to Mo^{5+} (232.1 eV), and the extent of this reduction increases when Pt and Ru are incorporated to PRMO. For the $MoCl_5$ precursor the most intense $Mo3d_{5/2}$ line was satisfactorily fitted to two components: a major one at 232.1 eV belonging to Mo^{5+} and a minor one at 232.8 eV associated to Mo^{6+}, originated from hydrolyzed $MoCl_5$ species still present in the $MoCl_5$ precursor, which indeed increases in MoCl/C. Interestingly, the incorporation of Pt and Ru over MoCl/C support results in a catalyst with only Mo^{5+} species. Besides, the Mo $3d_{5/2}$ line of Mo 3d doublet of the ammonium molybdate displayed a major Mo^{6+} component at 232.8 eV which decreases in MoNH/C support and especially during the synthesis of PRMNH. Therefore the binding energies of Mo3d levels point to the fact that incorporation of PtRu over MoNH/C and MoCl/C supports generates mainly Mo phases with oxidation states of Mo^{5+} and some contribution of Mo^{6+} in the case of PRMNH while the PRMO catalyst shows the highest percentage of Mo^{6+} (>50%). In addition, the Pt:Ru:Mo atomic ratio belonging to the topmost atomic layers, derived from XPS analysis, is similar to the bulk ratios calculated from TXRF data, and lower amount of metals on the surface of PRMNH are detected compared with PRMCl catalyst.

3.2. Electrocatalytic measurements

Fig. 5 depicts stable cyclic voltammograms of the Vulcan XC 72R and supports Mo/C in 0.5 M H_2SO_4 at 25 °C. The voltage is cycled between 0.02 and 1.25 V with a ramp rate equal to 0.02 V s^{-1}. The evolution of the voltammetric profiles shows a slight decrease of the peaks in MoCl/C and MoNH/C, related to the reduction–oxidation reactions of Mo, while high Mo losses are observed in MoO/C, suggesting that MoO_3 is dissolved to the electrolyte. In agreement with earlier studies [27,28] the Mo/C voltammogram exhibits a major peak at ca. 0.6 V, which is attributed to the oxidation of Mo^{4+} or Mo^{5+} to Mo^{6+}. In addition to this peak, and specifically in MoO/C, oxidation peaks were detected at ca. 0.1, 0.25 and 0.5 V, which correspond to a reduction of different MoO_x suboxides. The proportion of these Mo phases varies depending on the preparation procedure and pre-

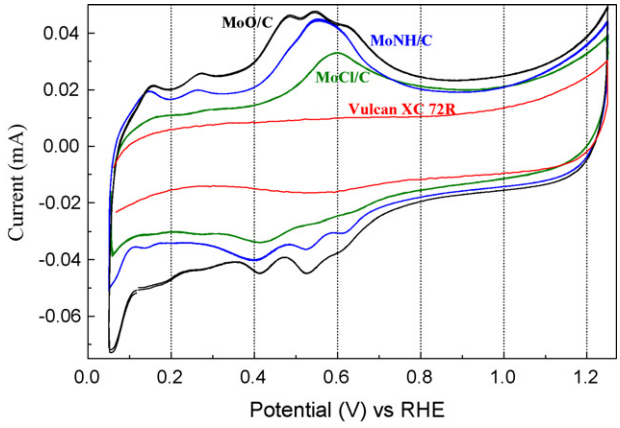

Fig. 5. CV of Vulcan XC 72R and Mo/C supports in 0.5 M H_2SO_4 at 25 °C. v = 0.01 V s^{-1}.

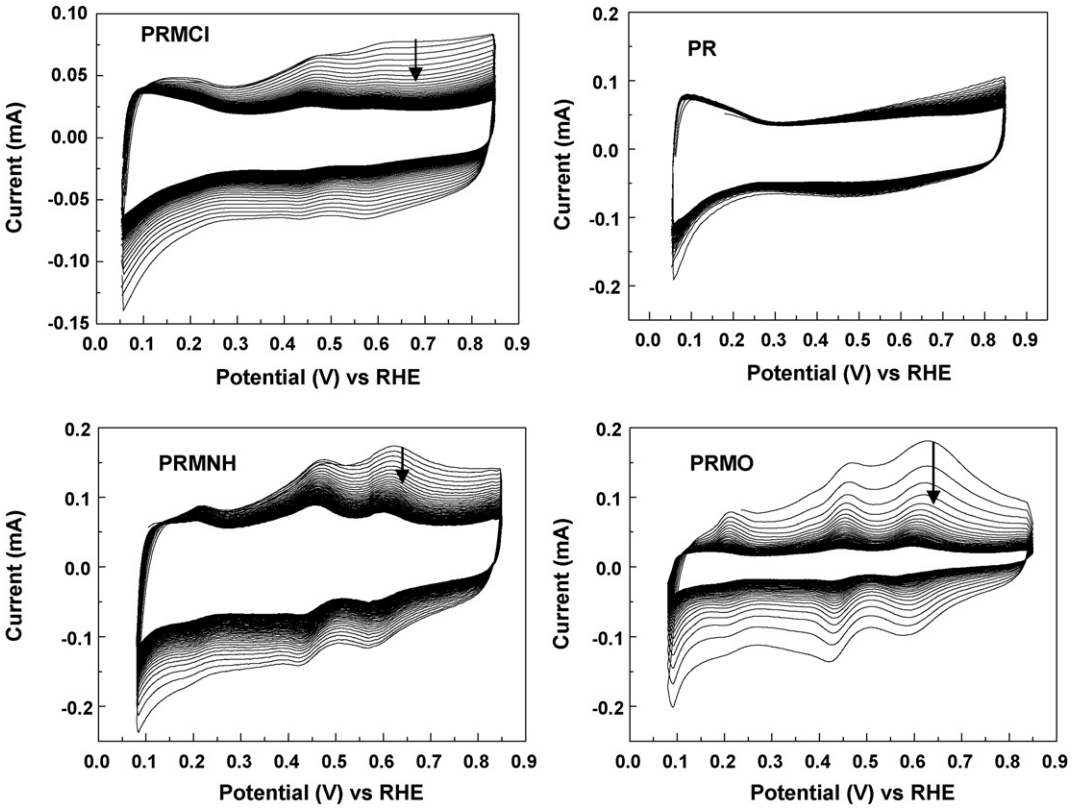

Fig. 6. CV of electrocatalysts in 0.5 M H_2SO_4 at 25 °C. $\nu = 0.01$ V s^{-1}.

cursor, since apparently these variables strongly influence the homogeneity and, hence, the surface composition of the Mo/C support.

The evolution of the voltammetric profiles of binary and ternary catalysts upon cycling in 0.5 M H_2SO_4 is shown in Fig. 6. PR catalyst shows the characteristic cyclic voltammogram of PtRu catalysts without any peak in the 0.25–0.8 V region. The current decrease observed in the curves after several cyclic voltammograms (50 scans) is attributed to some RuO_2 dissolution and some contaminated surface catalyst with sulfito complex. In all ternary systems a gradual decrease of the peaks between 0.4 and 0.6 V, related to the reduction–oxidation reactions of Mo, is evident, suggesting that Mo dissolves into the electrolyte. Quantitative differences in the rate of the Mo dissolution from PRMO, PRMCl and PRMNH catalysts by the shape of the cyclic voltammogram catalysts become apparent from the comparison of the voltammetric profiles, where PRMO shows the most important decrease of the peaks. The fact of Mo dissolution has been confirmed in a test by TXRF analysis (Table 3). When the electrochemical surface of catalysts remained stable under acidic conditions, i.e. the characteristics of the peaks (peak potential, peak height, peak width) do not change after 10 scans, electrocatalysts were removed from the electrode surface and the bulk composition was analyzed. It was observed that ternary catalysts display a dramatic loss of Ru and Mo metals, especially Mo, while minor loss of Ru was observed in binary catalyst. It seems that some Ru–Mo interaction take place, which facilitates the Ru dissolution. PRMNH is somewhat the most stable ternary catalyst.

Table 3
Bulk composition of catalyst after stability test.

Catalysts	Atomic ratio Pt:Ru:Mo
PRMCl	1:0.24:0.05
PRMNH	1:0.35:0.27
PRMO	1:0.05:0.11
PR	1:0.6

Beyond the H_2 oxidation, three apparent oxidation peaks appear at 0.2, 0.45 and 0.6 V in all ternary catalysts, though they are less evident in PRMCl. The respective reduction peaks are observed along the cathodic sweep of the voltammograms. Therefore, once the catalysts have been stabilized in the electrode similar Mo species along catalysts surface tend to get in all PtRuMo catalysts. That is indicative that similar interaction between metal–support and metal–metal is likely developed in carbon supported PtRuMo nanoparticles at these potential conditions.

Previous studies on well-defined polycrystalline PtMo alloy electrodes [29] show that the chemistry of the Mo atoms in the surface (and near surface) is quite complex. Therefore, in the case of ternary PtRuMo catalysts only a tentative ascription of the peaks is possible allowing qualitative distinction between reduction–oxidation response of Pt, Ru and that of Mo. *In situ* XAS studies were conducted with the aim to identify the nature of surface species of PtMo/C catalysts [30]. The Mo K edge XANES spectra at 0.0 V showed that Mo is present as a hydrated oxide species with an approximated oxidation state of Mo^{5+}, and there is a change in the oxidation state of Mo from Mo^{5+} to Mo^{6+} at 0.54 V, which remains stable till 0.85 V. In our voltammetric results the redox couple observed at ca. 0.2 and 0.45 V do agree with the presence of Mo in an oxidation state between Mo^{5+} and Mo^{6+}. *Ex situ* XPS analyses of electrocatalysts confirms the presence of these species. Unfortunately, no detailed information on the surface composition and its dependence on potential have been reported for PtRuMo catalysts.

The extra peak between 0.60 and 0.65 V can be explained when the cyclic voltammogram of Mo/C support is taken into account (see Fig. 5). Mo/C voltammogram exhibits one of the major peaks at ca.

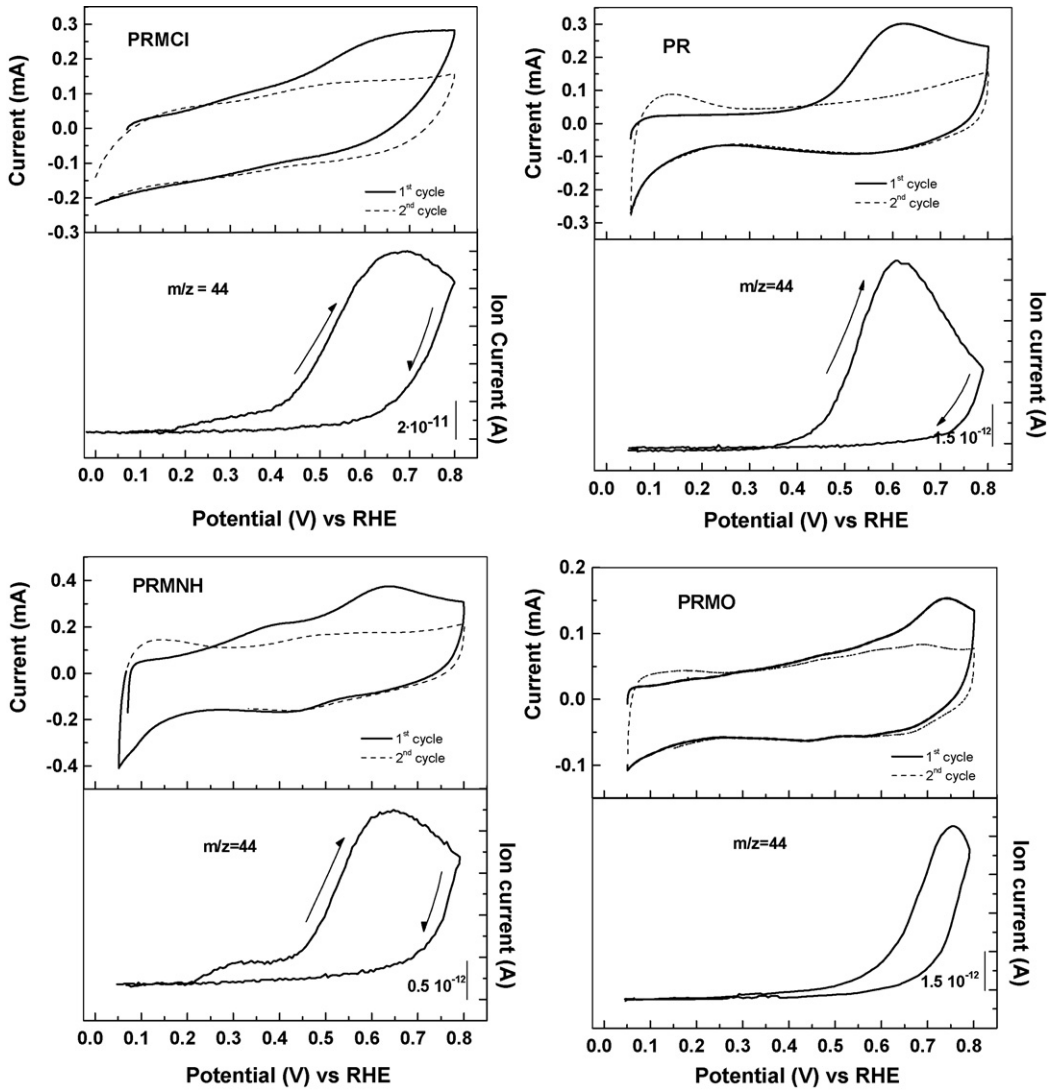

Fig. 7. CV for the oxidation of CO in 0.5 M H_2SO_4 at 25 °C of electrocatalysts and the corresponding signal for CO_2 production ($m/z = 44$). $\nu = 0.01\ V\ s^{-1}$.

0.6 V, indicating that non-alloyed carbon supported Mo undergoes a reduction–oxidation reaction in this potential region. Lebedeva and Janssen [31] reported cyclic voltammograms on PtMo/C and Mo/electrodes interfaced either with H_2SO_4 solutions or with Nafion membrane. They detected an oxidation peak at 0.65 V, which was attributed to isolated Mo species, and another peak at 0.45 V assigned to Mo atoms combined with Pt to form alloyed nanoparticles.

This suggests that for all catalysts investigated in the present work some pure non-alloyed Mo – most likely $MoO_3{\cdot}xH_2O$ – is present on the surface of carbon along with mixed Pt–Mo and/or RuMo phases. The poor stability of all PRMO in 0.5 M H_2SO_4 is directly related to the amphoteric character of MoO_3, which readily dissolves at pH below 0 [19]. Different dissolution rates of the PtRuMo catalysts in a given electrolyte can be related to their homogeneity. As can be seen from the results (Fig. 6) in most cases, the peak at ca. 0.6 V decreases quicker than that at ca. 0.45 V, suggesting that the non-alloyed MoO_3 phase dissolves more rapidly than Mo from the mixed Pt–MoO_3 phase. Therefore, the stability of a given electrode material is directly related to the degree of mixing of the components, which strongly depends on the precursor salts.

The electrooxidation of CO adsorbed on electrocatalysts provides information about the capability of the material for CO oxidation. A low onset potential (E_{onset}) of CO oxidation indicates a good CO tolerance of the electrocatalyst. Exact determination of the onset of CO oxidation from the electrochemical current includes certain difficulties given the need for double-layer correction and sometimes the presence of other faradaic contributions. In this case, differential electrochemical mass spectrometry (DEMS) is more appropriate since no faradaic or double-layer corrections are needed. Fig. 7 depicts the CVs and simultaneously recorded MSCVs related to production of CO_2 ($m/z = 44$), corresponding to the cation radical $[CO_2]^{\bullet+}$ (DEMS analysis) during the electrooxidation of CO adsorbed on electrocatalysts at 25 °C. The curves indicate that PRMNH and PRMCl catalysts display a high CO tolerance, with the onset for CO_2 production being observed at potentials ca. to 0.2 V for PRMNH and 0.17 V for PRMCl, which represents a negative shift of about 0.15 V with respect to PR catalyst at the same temperature ($E_{onset} = 0.35$ V). The shape of the cyclic voltammograms related to production of CO_2 indicates a higher current density at potentials lower than 0.5 V in PRMNH, which implies that oxidation of CO occurs easily at the potentials of operation in a PEMFC and DMFC. The PRMO catalyst displays a less favorable behavior. The onset for CO_2 production ($E_{onset} = 0.29$ V) shifts 0.06 V to negative values with respect to the PR catalyst, and the potentials for maximum ion current (E_{peak}) is achieved at ca. 0.75 V.

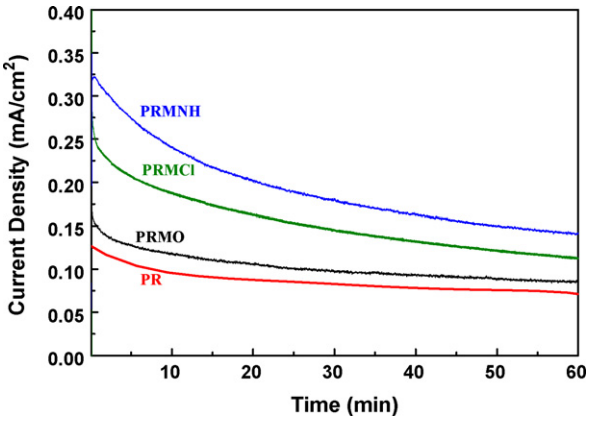

Fig. 8. Current–time curves towards methanol oxidation at 0.6 V of electrocatalysts in 2 M CH_3OH + 0.5 M H_2SO_4 at 25 °C. Current scale is normalized for the EAS estimated from CO_{ads} stripping voltammetry.

Fig. 8 shows current–time curves towards methanol oxidation for PRMNH, PRMCl, PRMO and PR at 25 °C in the Ar-saturated solution system of 2 M CH_3OH and 0.5 M H_2SO_4. It was observed that ternary catalysts perform better than the binary system, where the incorporation of a small amount of Mo significantly increases the intrinsic catalytic activity to methanol electrooxidation. In addition, the performance of the PRMNH is the best result obtained compared to the other samples prepared by the same method and from different precursors. The high current density towards methanol electrooxidation on the catalyst prepared with $(NH_4)_6Mo_7O_{24}$ corresponds to the superior CO tolerance of this catalysts. These results confirm that an important, although not unique, aspect of the catalysis of methanol oxidation is related to catalysis of CO oxidation.

Since factors, including the particle size and particle structure, have been excluded from causing the differentiation of the catalytic activity between PRMNH and PRMCl catalysts, the attention is drawn to their compositional homogeneity, metal oxidation states on surfaces and metal interactions. The results of the composition of the bulk after stability test show that some loss of Mo in the synthesis of PRMCl is evident (Table 3). Therefore, the use of $MoCl_5$ as precursor will be limited to the pH range in order to avoid a dramatic loss of Mo. However, the $(NH_4)_6Mo_7O_{24}$ precursor seems to be more stable and handy for synthesis of PtRuMo nanoparticles. Nevertheless, the precursor affect to the composition, which will be decisive in the activity.

The possible Pt–Mo and Ru–Mo interactions observed by cyclic voltammetries and TPR analysis are on one hand responsible for structural changes in the Mo oxides in PRMCl and PRMNH catalysts. These metal interactions promote its dissolution to the acid electrolyte, since such an effect although widely observed in the case of ternary catalysts was not observed to this extent in the Mo/C supports and PR catalyst. On the other hand, they are responsible for more active catalysts towards the CO_{ads} and methanol electrooxidation.

According to metal oxidation states of Mo, the catalysts that present the highest activity are at the same time the ones with the lower oxidation states of the Mo superficial species, and catalyst which proves the higher oxidation states of Mo (PRMO) not only result to high losses of metals during the stabilization of the system and lower activities, but at the same time affect negatively the Pt–Ru interactions. Accordingly, the CO_{ads} oxidation voltammetry of this catalyst is similar to a just Pt catalyst, although, the small amount of Ru and Mo observed in PRMO after stability test (Table 3) seems to be enough to display a good activity in the methanol electrooxidation.

These results clearly demonstrate the importance of the Mo precursor in the preparation procedure of ternary electrocatalyst PtRuMo/C and the fact that highly oxidized molybdenum phases are not desirable in this kind of systems.

4. Conclusions

The main conclusive remarks of this study can be summarized as follows:

- The final composition and homogeneity of the ternary catalysts depend greatly on the precursor used. $MoCl_5$ results in a dramatic loss of Mo, while $(NH_4)_6Mo_7O_{24}$ seems to be more stable and handy for synthesis of PtRuMo nanoparticles. However, similar structure and particle size are obtained in both PRMNH and PRMCl electrocatalysts.
- Once the catalysts have been stabilized, similar Mo species along the surface tend to get in all PtRuMo catalysts. That is indicative that similar metal–support and metal–metal interactions likely occurs in carbon supported PtRuMo nanoparticles at these potential conditions.
- Pt–Mo and Ru–Mo interactions that take place in PRMNH and PRMCl and the lower oxidation states of the Mo superficial species (Mo^{5+}) may be responsible of the higher activity in CO and methanol electrooxidation observed in these catalysts compared with PRMO.
- Both composition and Ru–Mo interactions detected by TPR can be responsible for the higher activity observed in PRMNH.
- Finally, the PRMO catalyst proves that the presence of high oxidation states of Mo^{6+} not only results to high losses of metals during the stabilization of the system, but at the same time affects negatively the formation of Pt–Ru interactions.

Acknowledgements

This research was funded by the Ministry of Science and Innovation, Spain (Projects ENE2007-67533-C02-01 and MAT2008-06631-C03-02/MAT). M.V.M.-H. acknowledges the Ramon y Cajal Program of the Ministry of Science and Innovation of Spain for financial support. N.T. acknowledges the I3P program (CSIC) for financial support.

References

[1] R. Borup, J. Meyers, B. Pivovar, Y.S. Kim, R. Mukundan, N. Garland, D. Myers, M. Wilson, F. Garzon, D. Wood, P. Zelenay, K. More, K. Stroh, T. Zawodzinski, J. Boncella, J.E. McGrath, M. Inaba, K. Miyatake, M. Hori, K. Ota, Z. Ogumi, S. Miyata, A. Nishikata, Z. Siroma, Y. Uchimoto, K. Yasuda, K. Kimijima, N. Iwashita, Chem. Rev. 107 (2007) 3904–3951.
[2] R. Rashidi, I. Dincer, G.F. Naterer, P. Berg, J. Power Sources 187 (2009) 509–516.
[3] O. Petrii, J. Solid State Electrochem. 12 (2008) 609–642.
[4] H. Liu, C. Song, L. Zhang, J. Zhang, H. Wang, D.P. Wilkinson, J. Power Sources 155 (2006) 95–110.
[5] M. Watanabe, S. Motoo, J. Electroanal. Chem. 60 (1975) 267–273.
[6] T. Frelink, W. Visscher, J.A.R. van Veen, Surf. Sci. 335 (1995) 353.
[7] T.Y. Morante-Catacora, Y. Ishikawa, C.R. Cabrera, J. Electroanal. Chem. 621 (2008) 103–112.
[8] S. Pasupathi, V. Tricoli, J. Solid State Electrochem. 12 (2008) 1093–1100.
[9] A. Bauer, E.L. Gyenge, C.W. Oloman, J. Power Sources 167 (2007) 281–287.
[10] D.C. Papageorgopoulos, M. Keijzer, F.A. de Bruijn, Electrochim. Acta 48 (2002) 197–204.
[11] Z. Hou, B. Yi, H. Yu, Z. Lin, H. Zhang, J. Power Sources 123 (2003) 116–125.
[12] A. Lima, C. Coutanceau, J.M. Leger, C. Lamy, J. Appl. Electrochem. 31 (2001) 379–386.
[13] M.V. Martínez-Huerta, J.L. Rodríguez, N. Tsiouvaras, M.A. Peña, J.L.G. Fierro, E. Pastor, Chem. Mater. 20 (2008) 4249–4259.
[14] A.B. Anderson, E. Grantscharova, S. Seong, J. Electrochem. Soc. 143 (1996) 2075–2082.
[15] Z. Ji, A.F. Jalbout, J.Q. Li, Solid State Commun. 142 (2007) 148–153.
[16] J. Horkans, M.W. Shafer, J. Electrochem. Soc. 124 (1977) 1196–1202.
[17] N. Tsiouvaras, M.V. Martínez-Huerta, R. Moliner, M.J. Lázaro, J.L. Rodríguez, E. Pastor, M.A. Peña, J.L.G. Fierro, J. Power Sources 186 (2009) 299–304.

[18] M. Watanabe, M. Uchida, S. Motoo, J. Electroanal. Chem. 229 (1987) 395–406.
[19] A.F. Holleman, E. Wiberg, Inorganic Chemistry, Academic Press, 2001, pp. 1382–1402.
[20] H.A. Gasteiger, P.N. Ross, E.J. Cairns, Surf. Sci. 32 (1993) 168.
[21] J. Haber, E. Lalik, Catal. Today 33 (1997) 119–137.
[22] J.L. Gómez de la Fuente, M.V. Martínez-Huerta, S. Rojas, P. Hernández-Fernández, P. Terreros, J.L.G. Fierro, M.A. Peña, Appl. Catal. B: Environ. 88 (2009) 505–514.
[23] B.S. Hobbs, A.C.C. Tseung, Nature 222 (1969) 556–558.
[24] G.C. Bond, J.B.P. Tripathi, J. Chem. Soc. Faraday Trans. I 72 (1976) 933.
[25] D. Briggs, M.P. Seah, Practical Surface Analysis by Auger and X-ray Photoelectron Spectroscopy, 1990.
[26] A.S. Arico, V. Baglio, A. Di Blasi, E. Modica, P.L. Antonucci, V. Antonucci, J. Electroanal. Chem. 557 (2003) 167–176.
[27] E.I. Santiago, G.A. Camara, E.A. Ticianelli, Electrochim. Acta 48 (2003) 3527–3534.
[28] E.I. Santiago, M.S. Batista, E.M. Assaf, E.A. Ticianelli, J. Electrochem. Soc. 151 (2004) A944–A949.
[29] B.N. Grgur, N.M. Markovic, P.N. Ross, J. Electrochem. Soc. 146 (1999) 1613–1619.
[30] S. Mukerjee, R.C. Urian, Electrochim. Acta 47 (2002) 3219–3231.
[31] N.P. Lebedeva, G.J.M. Janssen, Electrochim. Acta 51 (2005) 29–40.